High-Performance Hybrid Supercapacitor Enabled by a High-Rate Si-based Anode

*Ran Yi, Shuru Chen, Jiangxuan Song, Mikhail L. Gordin, Ayyakkannu Manivannan, and Donghai Wang**

A hybrid supercapacitor constructed of a Si-based anode and a porous carbon cathode is demonstrated with both high power and energy densities. Boron-doping is employed to improve the rate capability of the Si-based anode (B-Si/SiO_2/C). At a high current density of 6.4 A/g, B-Si/SiO_2/C delivers a capacity of 685 mAh/g, 2.4 times that of the undoped Si/SiO_2/C. Benefiting from the high rate performance along with low working voltage, high capacity, and good cycling stability of B-Si/SiO_2/C, the hybrid supercapacitor exhibits a high energy density of 128 Wh/kg at 1229 W/kg. Even when power density increases to the level of a conventional supercapacitor (9704 W/kg), 89 Wh/kg can be obtained, the highest values of any hybrid supercapacitor to date. Long cycling life (capacity retention of 70% after 6000 cycles) and low self-discharge rate (voltage retention of 82% after 50 hours) are also achieved. This work opens an avenue for development of high-performance hybrid supercapacitors using high-performance Si-based anodes.

1. Introduction

The expanding market of portable electronic devices and, especially, the emergence of electric vehicles (EV) and hybrid electric vehicles (HEV) have created increasing demand for advanced energy storage techniques that can provide high energy and power densities and long cycling life.[1,2] In today's practical applications, the two major energy storage systems are lithium-ion batteries (LIBs) and supercapacitors (SCs), which represent two extremes of the design space. LIBs can deliver high energy densities (150–250 Wh/kg) by utilizing Faradaic reactions throughout the active materials.[3] However, this mechanism leads to low power densities (<1000 W/kg) since solid-state ion diffusion in bulk electrodes is generally slow.[3,4] LIBs also suffer from short cycling lives (<1000 cycles) due to degradation of material structures.[5] On the opposite extreme, SCs offer high power densities (≈10 000 W/kg) because of the fast physical sorption rates of charges on the surfaces of active materials.[3,6] This mechanism also enables long cycling lives (>100 000 cycles), since it does not cause major structural changes.[7] However, as only the surface is utilized, the energy densities of SCs are very limited (5–10 Wh/kg).[7,8] In view of the issues of current LIBs and SCs, it is highly desirable, but also very challenging, to develop an energy storage system with high energy and power densities and long cycling life by combining the advantages of both LIBs and SCs.

Hybrid supercapacitors or supercapacitor–battery hybrid energy storage systems have been proposed as a way to incorporate the advantages of both LIBs and SCs into one system.[9–11] Such systems usually consist of SC electrodes (activated carbon) as cathodes to ensure high power density through adsorption/desorption of anions and LIB electrodes as anodes to provide high energy density by lithium insertion/extraction in a non-aqueous electrolyte (**Figure 1**).[12] Various examples of such systems have been reported with encouraging results.[5,9–11,13–17] For example, Zhang et al. demonstrated the highest energy density to date (147 Wh/kg at 150 W/kg) by coupling a graphene-based three-dimensional porous carbon cathode and a Fe_3O_4/graphene nanocomposite anode.[13] However, in most of these reports, high energy densities are only achieved at very low power densities, and energy densities decrease significantly with increasing power densities. A system with high energy density at high power density, along with long cycling life, has not yet been demonstrated. This is largely due to a lack of high performance anodes. Assuming a strictly linear charge/discharge slope without voltage drop, the energy and power densities can be calculated by the following equations:

$$E = \frac{1}{2}(V_1 + V_2)I\Delta t \quad (1)$$

$$P = \frac{E}{\Delta t} \quad (2)$$

where E, P, V_1, V_2, I, and Δt are the energy density, power density, lower and upper limits of the voltage window, current density, and discharge duration, respectively.[15,18] According to these equations, to achieve high energy and power densities requires high operating voltage (V_1 + V_2), high rate capability (which allows for high current density), and high capacity (which gives long discharge duration). Because the anode

R. Yi, S. Chen, Dr. J. Song, M. L. Gordin, Prof. D. Wang
Department of Mechanical and Nuclear Engineering
The Pennsylvania State University
University Park
PA 16802, USA
E-mail: dwang@psu.edu
Dr. A. Manivannan
US Department of Energy/NETL
3610 Collins Ferry Rd., Morgantown, WV 26507, USA

DOI: 10.1002/adfm.201402398

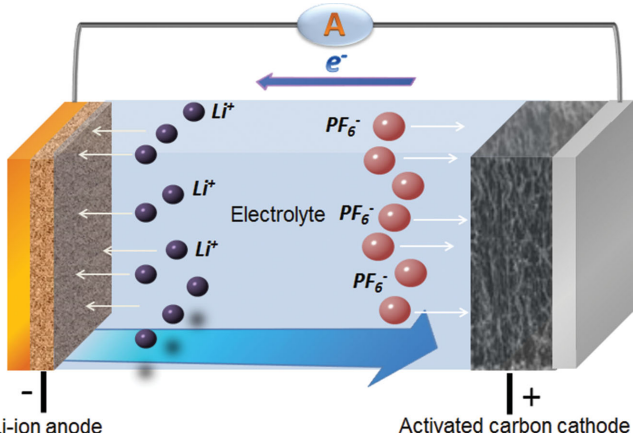

Figure 1. Charging process of a hybrid supercapacitor using activated carbon as the cathode and a Li-insertion material as the anode.

undergoes lithiation during charging of the hybrid supercapacitor, a lower anode lithiation voltage enables a higher V_2 and thus leads to higher energy and power densities if other parameters are unchanged. In addition, good anode cycling stability is indispensable for long cycling life of the hybrid supercapacitors, since Faradaic anodes usually suffer from shorter cycling lives compared to capacitive cathodes. Based on the analysis above, an ideal anode in a hybrid supercapacitor system should have the following features: 1) the working voltage should be low so that the system is able to fully utilize the voltage window of the electrolyte to enable high energy density; 2) the anode should have high specific capacity to increase the energy density; 3) the anode should have excellent rate capability to match the high-power cathode to achieve high power density; and 4) the cycling life should be long to improve cycling stability of the hybrid system. However, none of the anode materials used thus far in hybrid supercapacitors meet all these requirements. For example, $Li_4Ti_5O_{12}$ and TiO_2 have good cycling stability but high voltage (1.5 V) and low capacity (around 200 mAh/g).[4,8] Graphite, on the other hand, shows the lowest lithiation voltage (0.1 V) but low capacity (370 mAh/g) and mediocre rate performance.[6]

Silicon is a promising anode material candidate for hybrid supercapacitors because of its low lithiation potential (<0.5 V) and high specific capacity (>3500 mAh/g).[19,20] However, Si suffers from fast capacity fading caused by its large volume change (>300%) during lithiation/delithiation.[21] In addition, Si has low electronic conductivity due to its intrinsic semiconductor nature, which limits its rate capability.[22] Thus, preparing Si-based anodes with long cycling life and high power density is an essential requirement for Si-containing hybrid supercapacitors. Tremendous efforts have been made to solve these issues of Si-based anodes, frequently by designing Si nanostructures such as nanowires, nanotubes, nano and micro-sized particles.[23–29] However, preparation of most of these materials involves costly chemical/physical vapor deposition or highly toxic hydrofluoric acid (HF) etching. Herein, we report a hybrid supercapacitor with high energy and power densities enabled by a high-performance Si-based anode. The cycling stability and rate performance of the anode material were improved by size reduction, carbon coating, and boron doping of commercial silicon monoxide (SiO) without any HF etching. When used as a Li-ion battery anode, the resultant composite (B-Si/SiO_2/C) exhibits a capacity of 1279 mAh/g after 100 cycles at 0.6 A/g (92.7% capacity retention) and excellent high rate performance of 685 mAh/g at 6.4 A/g. Coupling this material with highly porous spherical carbon (PSC) creates a high-voltage hybrid supercapacitor (B-Si/SiO_2/C//PSC) operating between 2.0–4.5 V with a high energy density of 128 Wh/kg at 1229 W/kg. Even at a high power density of 9704 W/kg, 89 Wh/kg can be retained, the highest values of any hybrid supercapacitor to date. In addition, the hybrid supercapacitor shows good capacity retention of 70% after 6000 cycles at 1.6 A/g and a low self-discharge rate with voltage retention of 82% after 50 h.

2. Results and Discussion

Figure 2a shows the X-ray diffraction (XRD) patterns of B-Si/SiO_2/C and Si/SiO_2/C. Both patterns contain the peaks associated with crystalline Si (JCPDS Card No.27–1402) and amorphous SiO_2, formed by disproportionation of SiO during heat treatment of the samples.[30] The average size of Si nanocrystallites in both samples is estimated to be about 15 nm by the Debye–Scherrer equation. However, careful observation reveals a slight difference of Si peak positions between the two samples. The Si peaks of B-Si/SiO_2/C are at higher angles than those of Si/SiO_2/C due to the B-doped material having smaller lattice constants, indicating the replacement of Si atoms by smaller B atoms.[31,32] In addition, no peaks of Si–B alloy are observed, supporting that B is doped into the Si. The boron doping was further examined by X-ray photoelectron spectroscopy (XPS). As shown in Figure 2b, both a B–O peak (193 eV) and a weak B–B/B–Si peak (188/187 eV) are present, agreeing well with the previous study on B-doped Si nanocrystals embedded in a silicon dioxide matrix and serving as solid evidence of boron doping.[33] The content of B is calculated to be around 4% (atomic percentage) by XPS survey. Raman spectroscopy (Figure 2c) of B-Si/SiO_2/C shows two peaks at 1340 and 1605 cm^{-1} that are attributed to the D (disordered) and the G (graphite) bands of carbon, respectively, indicating the presence of carbon formed by thermal decomposition of acetylene.[28] The mass percentage of carbon in B-Si/SiO_2/C was found to be 3.5% by elemental analysis.

The morphology, size, and structure of B-Si/SiO_2/C were investigated by scanning electron microscopy (SEM) and transmission electron microscopy (TEM). As shown in the SEM image (Figure 2d), B-Si/SiO_2/C is composed of micro-sized particles with an average size of about 3 μm and sub-micrometer particles, much smaller than the size (20 μm, Figure S1 in Supporting Information) of the pristine SiO precursor before ball milling. The nanoscale structure of disproportionated SiO is shown in the high-resolution TEM (HRTEM) image (Figure 2e). Lattice fringes with a d-spacing of 0.31 nm can clearly be seen, corresponding to the (111) crystal planes of the Si. It is also clear that crystalline Si domains with size of around 15 nm are dispersed in an amorphous SiO_2 matrix, the latter of which could act as a buffer layer for volume change of Si during lithiation/delithiation and thus improve cycling stability.[34] Figure 2f shows the TEM image of B-Si/SiO_2/C,

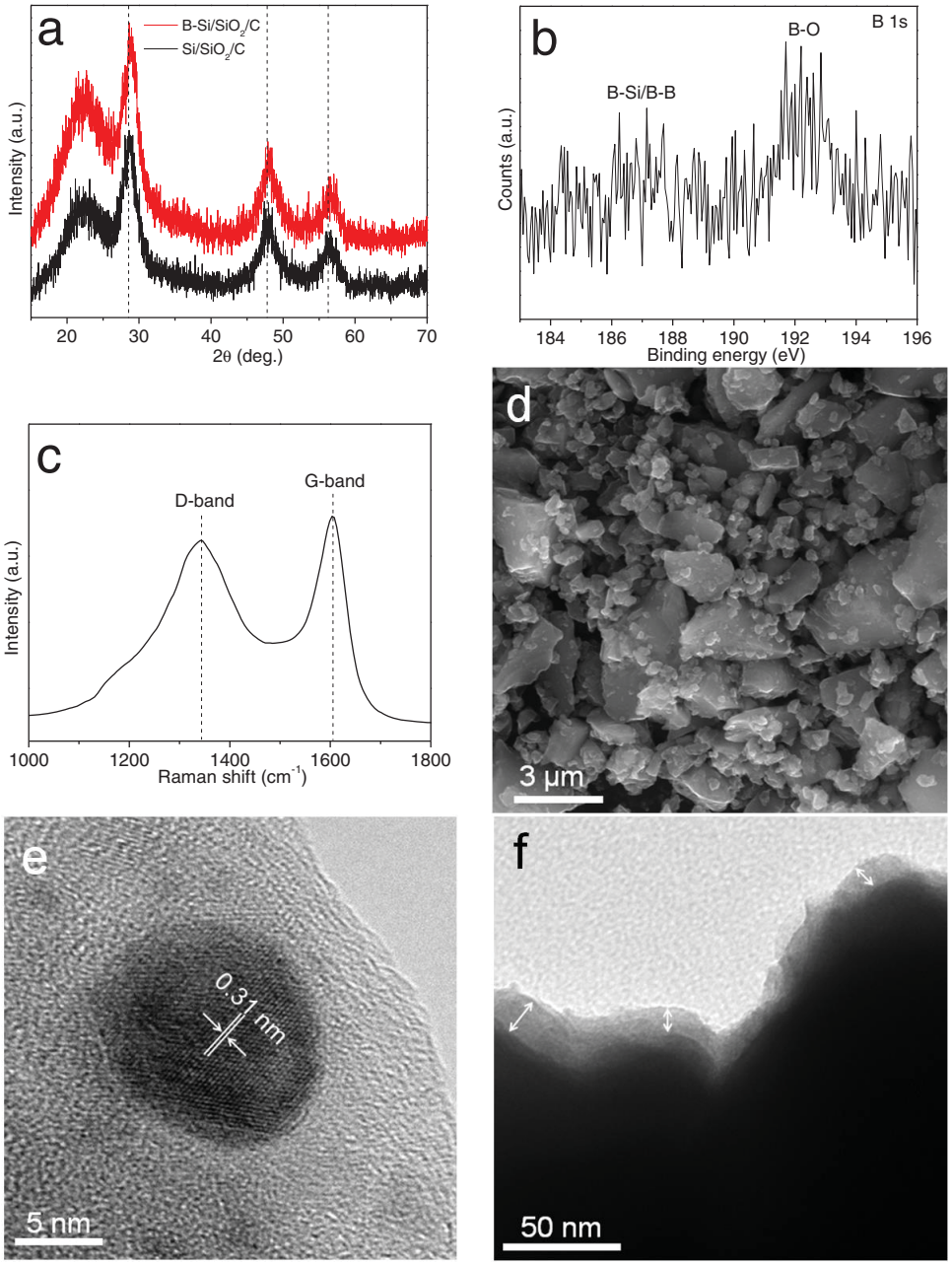

Figure 2. a) XRD patterns of B-Si/SiO_2/C and Si/SiO_2/C. b) B 1s XPS spectrum, c) Raman spectrum, and d) SEM image of B-Si/SiO_2/C. e) HRTEM image of B-Si/SiO_2. f) TEM image of B-Si/SiO_2/C.

in which the thickness of the carbon layer (marked by white arrows) was found to be around 20–30 nm. A low-magnification TEM showing overall morphology with the carbon layer is available in Figure S2 (Supporting Information).

The influence of size reduction of the SiO precursor and boron doping on the electrochemical performance of the resultant products was evaluated by galvanostatic cycling in Li-ion half-cells. For comparison, boron-doped Si/SiO_2/C using SiO which was not ball-milled (B-Si/SiO_2/C-325) and undoped Si/SiO_2/C using ball-milled SiO (Si/SiO_2/C) were prepared. These control samples have similar carbon content (3.5 wt%) to B-Si/SiO_2/C. **Figure 3**a shows the cycling performance of B-Si/SiO_2/C and B-Si/SiO_2/C-325 at a current density of 600 mA/g with the first two cycles activated at 300 mA/g. It is clear that B-Si/SiO_2/C exhibits better cycling stability than B-Si/SiO_2/C-325. A capacity of 1279 mAh/g was obtained by B-Si/SiO_2/C after 100 cycles, equating to 92.7% capacity retention (based on the lithiation capacity of the 3rd cycle), while B-Si/SiO_2/C-325 only delivered 990 mAh/g after 100 cycles, only 75% of its initial capacity. B-Si/SiO_2/C also has higher specific capacity during its first several cycles than B-Si/SiO_2/C-325, indicating that size reduction leads to short charge transport paths and thus increased material utilization. Another notable feature of B-Si/SiO_2/C is its high Coulombic efficiency (CE)

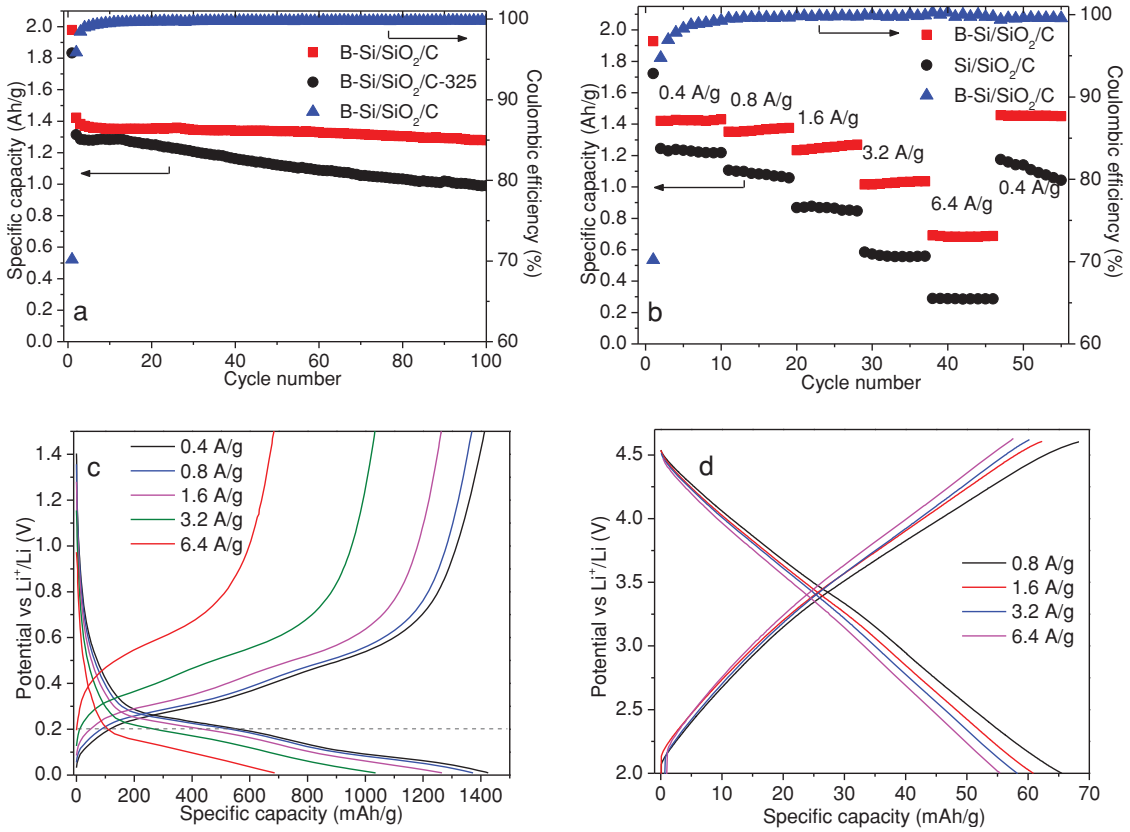

Figure 3. a) Cycling performance of B-Si/SiO_2/C and B-Si/SiO_2/C-325 at 600 mA/g, after the first two cycles of activation at 300 mA/g. b) Rate performance of B-Si/SiO_2/C and Si/SiO_2/C. Voltage profiles of c) B-Si/SiO_2/C and d) PSC at different current densities. Data are from tests in half-cell configuration with Li foil as counter electrodes.

during cycling. B-Si/SiO_2/C shows an acceptable first cycle CE of 71%. The CE quickly rises to 99.5% and 99.7% after 9 and 20 cycles, respectively, and thereafter remains at that level. The average CE from the 2nd to 100th cycle is 99.67%, which is rarely reported for Si-based anode materials. The doping effects on reduced-size Si/SiO_2/C were examined by charge/discharge at different current densities. As shown in Figure 3b, the difference in the specific capacities of doped and undoped ball-milled Si/SiO_2/C becomes more and more pronounced with increasing current density. At a high current density of 6.4 A/g, B-Si/SiO_2/C delivers a capacity of 685 mAh/g, 2.4 times that of Si/SiO_2/C (286 mAh/g). After the current density was restored to 400 mA/g, B-Si/SiO_2/C showed excellent reversibility, with a capacity similar to its initial capacity, while Si/SiO_2/C showed lower capacity and poor stability. The improved rate performance by boron doping is ascribed to a lower charge transfer resistance, as evidenced by electrochemical impedance spectroscopy (EIS) (Figure S3, Supporting Information). The B-Si/SiO_2/C has a smaller semicircle in the high-to-medium frequency region, which is generally ascribed to having a lower charge transfer resistance.[35] It is worth noting that the CE of B-Si/SiO_2/C remains around 99.7% even at high rates. Figure 3c shows voltage profiles of B-Si/SiO_2/C at different rates. A relatively flat lithiation plateau below 0.3 V can be observed in all profiles. A large portion of capacity is reserved even under lower voltage, for example, 0.2 V as marked by dash line. As an extreme, the capacity is 108 mAh/g when B-Si/SiO_2/C was lithiated to 0.2 V at 6.4 A/g, giving 577 mAh/g that could be used when lithiated B-Si/SiO_2/C is coupled as an anode in a hybrid supercapacitor. The large capacity reservoir at high current density, combined with the low voltage plateau, should enable a large voltage window in a hybrid supercapacitor.

Porous spherical carbon (PSC), which was reported in our previous work on lithium-sulfur batteries, was chosen as the cathode material.[36] The physical properties of PSC have been well characterized, featuring a hierarchical mesoporous structure with mesopores ranging from 5 to 25 nm in diameter, a high surface area of 1014 m^2/g, and a high pore volume of 2.5 cm^3/g.[36] The PSC was evaluated in a Li half-cell over a potential range of 2.0 to 4.6 V (Figure 3d). Capacities vary from 65 to 55 mAh/g at 0.8–6.4 A/g. Linear charge/discharge profiles were observed at all current densities, indicating capacitive behavior with the adsorption/desorption of ions on the surface.[3] The cyclic voltammetry (CV) curves (Figure S4, Supporting Information) also show quasi-rectangular shapes, close to the ideal capacitive behavior.

Based on the electrochemical characteristics of B-Si/SiO_2/C and PSC, the following guidelines were used for design and evaluation of the hybrid supercapacitor. B-Si/SiO_2/C was cycled 10 times at 400 mAh/g in a Li half-cell to achieve high efficiency and then lithiated to 0.2 V. Thereafter the lithiated B-Si/SiO_2/C electrode was coupled with a fresh PSC cathode to fabricate a

hybrid supercapacitor (B-Si/SiO_2/C//PSC). The mass ratio of PSC to B-Si/SiO_2/C was set at 2:1 to obtain long cycling life, as this left a fair margin of anode for gradual consumption of Si due to structural degradation during extended cycling.[29] The voltage window of 2.0–4.5 V was chosen to avoid both oxidative decomposition of electrolytes and possible Li intercalation into the carbon-based cathode (under 2.0 V, Figure S5, Supporting Information).[37,38]

The CV curves of the hybrid supercapacitor from 2.0 to 4.5 V are shown in **Figure 4**a. As the scan rate increased, the curves gradually deviated from the ideal rectangular shape due to the overlapping effects of capacitive behavior from the cathode and Faradaic behavior from anode. Figure 4b shows the voltage profiles at different current densities. Note that the current densities are based on the total mass of active material on both the cathode and the anode. The curves show little deviation from the linear slope of an ideal supercapacitor, which is due to the relatively flat charge/discharge plateau of the Si-based anode. The energy and power densities of the hybrid supercapacitor were calculated based on these curves and the results are shown in Figure 4c in comparison with energy densities at maximum power densities of each previous study. A high energy density of 128 Wh/kg can be achieved at a power density of 1229 W/kg. Even at an ultra-high power density of 9704 W/kg, which is on a par with conventional supercapacitors, the hybrid supercapacitor can still deliver 89 Wh/kg. To the best of our knowledge, such high energy and power densities have not been achieved by other hybrid supercapacitor systems. Given that the mass percentage of active materials in commercial energy storage devices is about 35–40%,[39] the gravimetric energy density of a device using this B-Si/SiO_2/C//PSC system could reach 32 Wh/kg at 3396 W/kg. In addition, such a device could have high volumetric energy and power densities thanks to the high tap densities of both PSC (0.5 g/cm^3) and B-Si/SiO_2/C (0.7 g/cm^3), which stem from their micrometer-scale particle size. Finally, one key advantage of supercapacitors over other energy storage techniques is their long-term cycling stability.[7] Figure 4d shows the cycling performance of the hybrid supercapacitor at 1.6 A/g. The capacity retention is 70% after 6000 cycles. The influence of voltage window on the performance of the hybrid supercapacitor was also investigated. A drop of 0.5 V in upper voltage limit (2.0 to 4.0 V) slightly decreases power densities but nearly halves energy densities while improves the cycling performance with a capacity retention of 77% after 6000 cycles (Figure S6 and Table S1 in Supporting Information). This clearly shows the importance of high upper voltage limit in improving energy densities of hybrid supercapacitors.

The self-discharge behavior of supercapacitors is one key concern for practical applications. Conventional supercapacitors suffer from a higher self-discharge rate than Li-ion batteries.[40,41] Incorporation of a Li-active anode in the hybrid

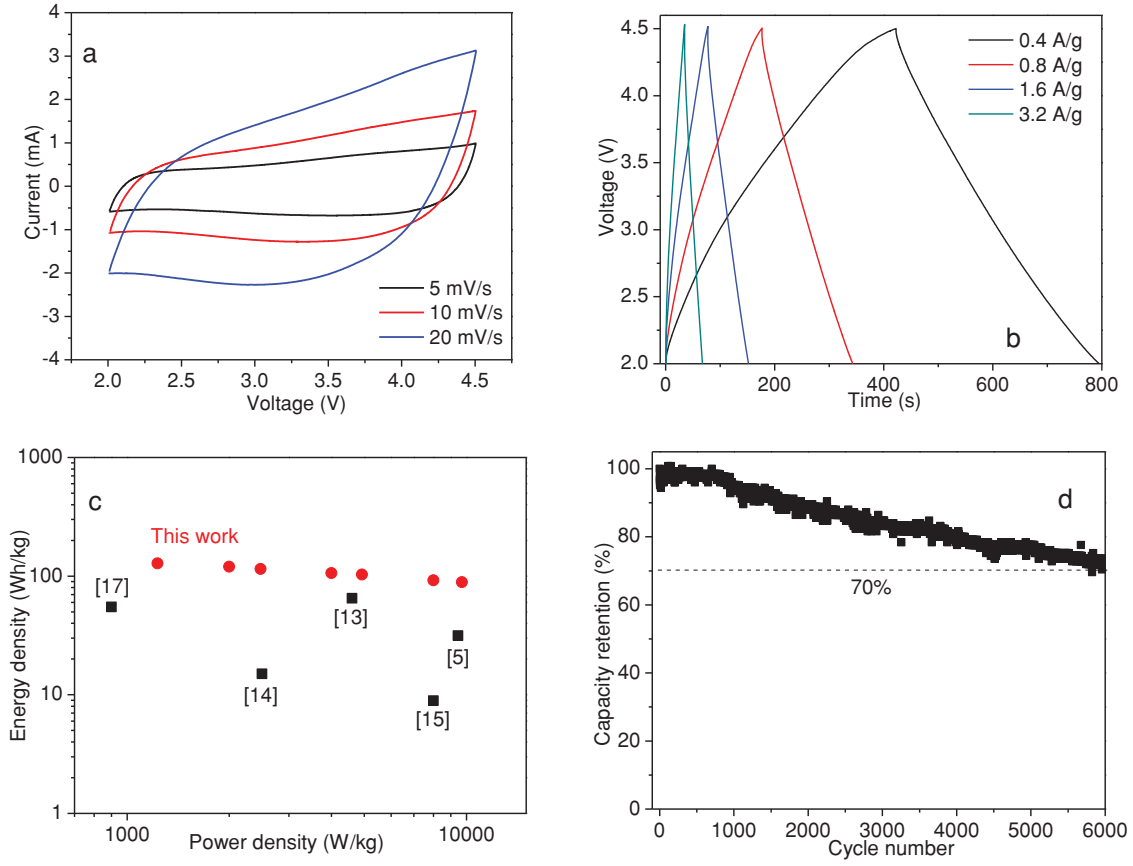

Figure 4. a) CV curves, b) galvanostatic charge–discharge curves, c) Ragone plot in comparison with energy densities at maximum power densities of other work, and d) cycling performance of the B-Si/SiO_2/C//PSC hybrid supercapacitor.

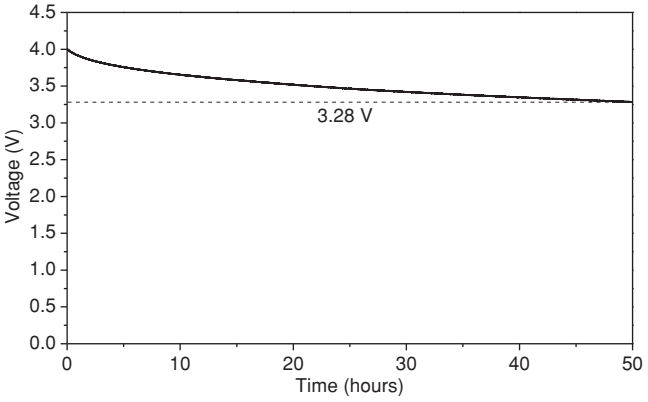

Figure 5. Self-discharge curve of the B-Si/SiO_2/C//PSC hybrid supercapacitor charged to 4.0 V at 100 mA/g followed by constant-voltage charging at 4.0 V for 1 h at room temperature.

supercapacitor was found to reduce the self-discharge rate. The hybrid supercapacitor was charged to 4.0 V at 100 mA/g, further charged at a constant potential of 4.0 V for 1 h, and then allowed to undergo self-discharge, all at room temperature. The open circuit voltage as a function of time was measured and is shown in **Figure 5**. The voltage dropped to 3.28 V over 50 h with a faster rate at the beginning, corresponding to 18% decay. This is much lower than those of the commercial high-voltage (3.5 V) supercapacitor (50% over 8 h) and the novel graphene-based micro-supercapacitors recently reported (50% over 13 h).[42]

3. Conclusion

In summary, we have designed a hybrid supercapacitor by coupling a porous carbon cathode and a high-performance Si-based anode. The Si-based anode has good cycling stability and rate performance, delivering a capacity of 685 mAh/g even at a high rate of 6.4 A/g. In addition, the low working voltage of Si grants the hybrid supercapacitor a high voltage window of 2.0–4.5 V. As a result, the hybrid supercapacitor exhibits a high energy density of 128 Wh/kg at 1229 W/kg. Even when power density increases to the level of a conventional supercapacitor (9704 W/kg), 89 Wh/kg can be obtained. Moreover, this system can achieve a long cycling life, with 70% capacity retention after 6000 cycles. The hybrid supercapacitor also features a low self-discharge rate, with voltage retention of 82% after 50 h. The present findings demonstrate that incorporating high-performance Si-based anodes is an effective approach to boost the energy and power densities of hybrid supercapacitors.

4. Experimental Section

Synthesis of Boron-doped Si/SiO_2/C Composite: Commercially available SiO powder (325 mesh) from Aldrich was used as precursor. For size reduction, SiO powder was subject to planetary ball-milling for 12 h at a speed of 400 rpm. The boron-doping was carried out in a horizontal quartz tube. A mixture of SiO powder (325 mesh, Sigma Aldrich) and B_2O_3 powder (Alfa Aesar) with 20:1 molar ratio of Si:B was used as the starting material. In a typical process, high-purity Ar was introduced at a flow rate of 1500 sccm for 20 min to purge the system. Afterwards the flow rate was reduced to 100 sccm and the tube was heated to 950 °C with a ramping rate of 10 °C/min, and kept at 950 °C for 5 h. The samples were taken out of the tube at temperatures below 40 °C. Carbon coating was done by thermal decomposition of acetylene gas at 700 °C for 30 min in a quartz furnace. The mixture of acetylene and high-purity argon (argon: acetylene = 9:1 by volume) is introduced at a flow rate of 100 sccm.

Synthesis of PSC Microspheres: PSC microspheres were prepared according to our previous report.[36]

Characterization: The obtained samples were characterized on a Rigaku Dmax-2000 X-ray powder diffractometer (XRD) with Cu Kα radiation (λ = 1.5418 Å). The operating voltage and current were kept at 40 kV and 30 mA, respectively. The size and morphology of the as-synthesized products were determined by a JEOL-1200 transmission electron microscope (TEM), FEI Nova NanoSEM 630 scanning electron microscope (SEM) and JEOL-2010F high-resolution transmission electron microscope (HRTEM). X-ray photoelectron spectroscopy (XPS) was conducted with a Kratos Analytical Axis Ultra XPS. Raman spectroscopy was conducted with a WITec CMR200.

Electrochemical Measurements: The electrochemical experiments were performed using 2016-type coin cells, which were assembled in an argon-filled dry glovebox (MBraun, Inc.). For half-cell testing, PSC and B-Si/SiO_2/C electrodes were used as the working electrodes and the Li metal was used as the counter and reference electrode. PSC electrodes were prepared by casting a slurry consisting of 80 wt% of active material, 10 wt% of Super P carbon black, and 10 wt% of polyvinylidene fluoride (PVDF) binder on carbon-coated aluminum foil. B-Si/SiO_2/C electrodes were prepared by mixing 70 wt% of active material, 15 wt% of Super P carbon black, and 15 wt% of poly(acrylic acid) (PAA) binder. 1 mol/L $LiPF_6$ in a mixture of ethylene carbonate, diethyl carbonate and dimethyl carbonate (EC: DEC: DMC, 2:1:2 by vol.) and 10 wt% fluoroethylene carbonate (FEC) was used as the electrolyte (Novolyte Technologies, Independence, OH). The hybrid supercapacitor was fabricated by coupling a prelithiated B-Si/SiO_2/C electrode (cycled 10 times, ending in a lithiated state at 0.2 V) and a fresh PSC electrode. The mass ratio of PSC to B-Si/SiO_2/C is 2:1. The mass loadings of active materials in the cathode and anode electrodes are 4 and 2 mg/cm^2, respectively. The electrochemical performance was evaluated by galvanostatic charge/discharge cycling on an Arbin BT-2000 battery tester at room temperature under different current densities. The voltage ranges for the PSC electrode and the B-Si/SiO_2/C electrode were 2.0–4.5 V and 0.01–1.5 V versus Li^+/Li, respectively. The hybrid supercapacitor was measured in the voltage range between 2.0 and 4.5 V. The current density was calculated based on the total mass of active materials on both the cathode and the anode. Cyclic voltammetry (CV) measurements were carried out on a Solartron SI 1287 electrochemical interface. Electrochemical impedance spectroscopy (EIS) was carried out by applying a perturbation voltage of 5 mV between 10 mHz and 100 kHz using a Solartron SI 1260 impedance analyzer. The energy density and power density of the hybrid supercapacitor were calculated according to the following equations:

$$E = \int_{t_1}^{t_2} IV\,dt \tag{3}$$

$$P = \frac{E}{t_2 - t_1} \tag{4}$$

where E (Wh/kg), V (V), I (A/kg), t_1 and t_2 (h), and P (W/kg) are the energy density, voltage, constant current density, discharge start and end time, and power density, respectively.

Supporting Information

Supporting Information is available from the Wiley Online Library or from the author.

Acknowledgements

This work was supported by the Assistant Secretary for Energy Efficiency and Renewable Energy, Office of Vehicle Technologies of the U.S. Department of Energy under Contract No. DE-AC02–05CH11231, Subcontract NO. 6951378 under the Batteries for Advanced Transportation Technologies (BATT) Program.

Received: July 18, 2014
Revised: August 14, 2014
Published online: September 22, 2014

[1] M. Armand, J. M. Tarascon, *Nature* **2008**, *451*, 652.
[2] M. S. Whittingham, *Chem. Rev.* **2004**, *104*, 4271.
[3] P. Simon, Y. Gogotsi, *Nat. Mater.* **2008**, *7*, 845.
[4] S. W. Lee, N. Yabuuchi, B. M. Gallant, S. Chen, B.-S. Kim, P. T. Hammond, Y. Shao-Horn, *Nat. Nanotechnol.* **2010**, *5*, 531.
[5] Y. Cai, B. Zhao, J. Wang, Z. Shao, *J. Power Sources* **2014**, *253*, 80.
[6] J. R. Miller, P. Simon, *Science* **2008**, *321*, 651.
[7] A. G. Pandolfo, A. F. Hollenkamp, *J. Power Sources* **2006**, *157*, 11.
[8] P. Simon, Y. Gogotsi, B. Dunn, *Science* **2014**, *343*, 1210.
[9] A. D. Pasquier, I. Plitz, J. Gural, S. Menocal, G. Amatucci, *J. Power Sources* **2003**, *113*, 62.
[10] G. G. Amatucci, F. Badway, A. Du Pasquier, T. Zheng, *J. Electrochem. Soc.* **2001**, *148*, A930.
[11] V. Khomenko, E. Raymundo-Piñero, F. Béguin, *J. Power Sources* **2008**, *177*, 643.
[12] B. E. Conway, W. G. Pell, *J. Solid State Electrochem.* **2003**, *7*, 637.
[13] F. Zhang, T. Zhang, X. Yang, L. Zhang, K. Leng, Y. Huang, Y. Chen, *Energy Environ. Sci.* **2013**, *6*, 1623.
[14] H. Kim, K.-Y. Park, M.-Y. Cho, M.-H. Kim, J. Hong, S.-K. Jung, K. C. Roh, K. Kang, *ChemElectroChem* **2014**, *1*, 125.
[15] H. Kim, M.-Y. Cho, M.-H. Kim, K.-Y. Park, H. Gwon, Y. Lee, K. C. Roh, K. Kang, *Adv. Energy Mater.* **2013**, *3*, 1500.
[16] S.-B. Ma, K.-W. Nam, W.-S. Yoon, X.-Q. Yang, K.-Y. Ahn, K.-H. Oh, K.-B. Kim, *Electrochem. Commun.* **2007**, *9*, 2807.
[17] X. Liu, H.-G. Jung, S.-O. Kim, H.-S. Choi, S. Lee, J. H. Moon, J. K. Lee, *Sci. Rep.* **2013**, *3*, 3183.
[18] V. Aravindan, Y. L. Cheah, W. F. Mak, G. Wee, B. V. R. Chowdari, S. Madhavi, *ChemPlusChem* **2012**, *77*, 570.
[19] B. A. Boukamp, G. C. Lesh, R. A. Huggins, *J. Electrochem. Soc.* **1981**, *128*, 725.
[20] M. Winter, J. O. Besenhard, M. E. Spahr, P. Novák, *Adv. Mater.* **1998**, *10*, 725.
[21] L. Y. Beaulieu, K. W. Eberman, R. L. Turner, L. J. Krause, J. R. Dahn, *Electrochem. Solid-State Lett.* **2001**, *4*, A137.
[22] T. Song, H. Cheng, H. Choi, J.-H. Lee, H. Han, D. H. Lee, D. S. Yoo, M.-S. Kwon, J.-M. Choi, S. G. Doo, H. Chang, J. Xiao, Y. Huang, W. I. Park, Y.-C. Chung, H. Kim, J. A. Rogers, U. Paik, *ACS Nano* **2011**, *6*, 303.
[23] A. Magasinski, P. Dixon, B. Hertzberg, A. Kvit, J. Ayala, G. Yushin, *Nat. Mater.* **2010**, *9*, 461.
[24] H. Wu, G. Chan, J. W. Choi, I. Ryu, Y. Yao, M. T. McDowell, S. W. Lee, A. Jackson, Y. Yang, L. Hu, Y. Cui, *Nat. Nanotechnol.* **2012**, *7*, 310.
[25] L.-F. Cui, Y. Yang, C.-M. Hsu, Y. Cui, *Nano Lett.* **2009**, *9*, 3370.
[26] B. M. Bang, J.-I. Lee, H. Kim, J. Cho, S. Park, *Adv. Energy Mater.* **2012**, *2*, 878.
[27] H. Kim, B. Han, J. Choo, J. Cho, *Angew. Chem. Int. Ed.* **2008**, *47*, 10151.
[28] R. Yi, F. Dai, M. L. Gordin, S. Chen, D. Wang, *Adv. Energy Mater.* **2013**, *3*, 295.
[29] R. Yi, F. Dai, M. L. Gordin, H. Sohn, D. Wang, *Adv. Energy Mater.* **2013**, *3*, 1507.
[30] M. Mamiya, M. Kikuchi, H. Takei, *J. Cryst. Growth* **2002**, *237–239*, Part 3, 1909.
[31] R. Yi, J. Zai, F. Dai, M. L. Gordin, D. Wang, *Electrochem. Commun.* **2013**, *36*, 29.
[32] J. M. Baribeau, S. J. Rolfe, *Appl. Phys. Lett.* **1991**, *58*, 2129.
[33] X. J. Hao, E. C. Cho, C. Flynn, Y. S. Shen, G. Conibeer, M. A. Green, *Nanotechnology* **2008**, *19*, 424019.
[34] X. Feng, J. Yang, Q. Lu, J. Wang, Y. Nuli, *Phys. Chem. Chem. Phys.* **2013**, *15*, 14420.
[35] E. Pollak, G. Salitra, V. Baranchugov, D. Aurbach, *J. Phys. Chem. C* **2007**, *111*, 11437.
[36] T. Xu, J. Song, M. L. Gordin, H. Sohn, Z. Yu, S. Chen, D. Wang, *ACS Appl. Mater. Interfaces* **2013**, *5*, 11355.
[37] K. Xu, *Chem. Rev.* **2004**, *104*, 4303.
[38] M. Schroeder, M. Winter, S. Passerini, A. Balducci, *J. Electrochem. Soc.* **2012**, *159*, A1240.
[39] H. S. Choi, J. H. Im, T. Kim, J. H. Park, C. R. Park, *J. Mater. Chem.* **2012**, *22*, 16986.
[40] B. W. Ricketts, C. Ton-That, *J. Power Sources* **2000**, *89*, 64.
[41] B. E. Conway, W. G. Pell, T. C. Liu, *J. Power Sources* **1997**, *65*, 53.
[42] M. F. El-Kady, R. B. Kaner, *Nat. Commun.* **2013**, *4*, 1475.